submitted to Eur. Phys. J. AP

Molecular Dynamics simulations of palladium cluster growth on flat and rough graphite surfaces

Pascal Brault[1,a] and Guy Moebs[2,b]

[1] Groupe de Recherches sur l'Energétique des Milieux Ionisés, UMR6606 CNRS-Université d'Orléans BP 6744, 45067 Orléans Cedex 2, France
[2] Centre de Ressources Informatiques de Haute-Normandie, 745 Avenue de l'Université, 76800 Saint Etienne du Rouvray, France

Abstract. Parallel Molecular Dynamics simulations are conducted for describing growth on surfaces with different kind of roughness : a perfect ordered crystalline flat graphite surface, a disordered rough graphite surface and flat surface with an ordered localized defect. It is shown that disordered rough surfaces results in a first step to reduction of the sticking coefficient, increased cluster density, size reduction. Structure of the clusters shows the disappearance of the octaedral site characteristic of compact structure. Isolated defect induces cluster-cluster interactions that modify growth compared to perfect flat surface. Kinetic study of growth shows power law $t^{\alpha z}$ evolution for low impinging atom kinetic energy. Increasing kinetic energy, on all kinds of surfaces, results in a slightly larger exponent z, but fitting by an exponential function is quite good too. Lattice expansion is favoured on rough surfaces but increasing incoming atom kinetic energy weakens this effect.

PACS. 81.15.Cd Deposition by sputtering – 81.15.Aa Theory and models of thin film growth – 68.55.Ac Nucleation and growth: microscopic aspects

1 Introduction

Cluster growth is a very important step in the early stages of thin film deposition [1]. Modern methods are emerging for depositing atoms in high non equilibrium situation such as pulse laser deposition [2], ion beam assisted deposition [3], plasma sputter deposition with high ion to neutral flux ratios [4,5,6]. The common feature of all these methods is the ability to ensure deposition assisted by ion flux and with varying and controlled kinetic energy of the depositing species. Moreover, the ions impinging the surface can be responsible for additional effects at the surface, i.e. creation of defects, film densification. Ion or plasma surface treatment can also be chosen for creating roughness expected to be suitable for thin film adhesion [7]. Some theoretical attempts have been undergone for modelling thin film deposition due to the availability of high performance computers [8,9,10]. In this context, an interesting feature that we describe here is the understanding of the role of ions and high kinetic energies have on the nucleation and growth of thin film, especially us-

ing Molecular Dynamics (MD) simulations [11,12,13,14, 15,16,17,18]. Main interest in MD is to carry precise calculations, provided that potential interactions are known, and to give deep insight into dynamical process [19]. Especially cluster growth of transition metal element such as Pd, Pt, Rh, Ni, Cu, ... is subject to many studies of the potential due to the interest in catalysis. So they fall within the capability of MD simulations because of the availability of now good interactions potentials issued from Embedded Atom Method (EAM) [20] or Tight Binding - Second Moment Approximation (TB-SMA) [22]. Both are true N-body potentials and are analytical. TB-SMA potentials are preferred on the basis of discussion in Ref. [21, 22,23]. This article is intended to examine how deposition conditions like kinetic energy of incoming atoms, defects or roughness of the virgin surface play a role in the cluster growth. Such a study is expected to be suitable for describing growth in plasma sputtering or pulsed laser deposition. Indeed, calculating sticking coefficients, radial density functions and statistical informations issued from snapshots of the surface will give relevant informations about initial steps of growth via clusters. So the present calculations are intended to show how cluster growth is dependant on the nature of roughness how kinetic energy

---

[a] e-mail: Pascal.Brault@univ-orleans.fr
[b] e-mail: Guy.Moebs@crihan.fr

of incoming atoms can minimize or not roughness effects. For this purpose we simulate the growth of palladium on three kinds of surfaces : a perfect ordered crystalline flat graphite surface, a disordered rough graphite surface and flat surface with an ordered localized defect. The next section will describe both the MD algorithm and the interaction potentials involved in the calculations. The results will be presented and discussed in the third section. The overall work will be summarized in the concluding section.

2 Molecular Dynamics

Molecular Dynamics (MD) is a simulation technique in which classical equations of motion are solved for a set of atoms or molecules. This leads to the well-known classical Newton set of equations describing the motion of atoms. This can be written in the form :

$$m_i \frac{\partial^2}{\partial t^2} \boldsymbol{r}_i = \sum_\lambda \boldsymbol{F}_i(\lambda) \qquad (1)$$

where m_i is the mass of the ith incoming atom interacting through the the forces $\boldsymbol{F}_i(\lambda)$. λ stands for surface atoms and adsorbed atoms . In principle we should have the same set of equations for the surface atoms: they interact among themselves and also with adsorbed atoms. In the following, the surface atoms remain at their initially fixed pos-including particle interactions with surface atomsitions. This is justified here for two reasons : first, graphite lattice is a very rigid lattice, second, impinging atom energies are well below graphite carbon displacement energy. The disordered surface is obtained by randomly displacing the atoms from their known equilibrium sites. When substrate atoms do not move, it is necessary to find a way for dissipating energy through the solid for allowing bonding to the surface. As a first attempt, we make use of quenched molecular dynamics [24]: if at a time step $\boldsymbol{F}.\boldsymbol{v} < 0$,($\boldsymbol{F}$ is the total force exerted on the considered atom), then the velocity $\boldsymbol{v}$ of the atoms is reset to a velocity randomly chosen in a velocity Maxwell distribution at surface temperature which is fixed here to $T_s = 300$ K (in Ref. [24], velocities are reset to 0). This is justified because the energy transfer considered here will not affect the graphite lattice due to its high stiffness. In that case, diffusion remains allowed and is random.

Simulating deposition needs to release atoms one after each other with a time delay Δt suitable for comparison with experiments, i.e. either the depositing atom flux reproduces exactly the one encountered in experiments or this time delay Δt is sufficient for allowing thermal relaxation of the already deposited atoms and/or thermal relaxation of surface atoms (when they are allowed to move). In our case we choose the latter asumption, which allows us to reduce computer time, even if it leads to large flux: this could be reasonable in sputter or pulsed laser deposition. Δt is thus fixed to 2 ps. Increasing this time delay does not change our results, which renders our assumption convenient.

Implementing suitable interatomic potentials is certainly the most important issue in molecular dynamics calculations. For describing transition metals like palladium, we use tight binding potential in the second moment approximation (TB-SMA)[22]. Such a potential is non pairwise in the sense that if atom i interact with atom j, the atoms surrounding atom j are explicitly taken into account.The TB-SMA force equation acting on atom i due to atom j surrounded by atoms k, can be written as :

$$\boldsymbol{F}_i(\text{Pd}-\text{Pd}) = \sum_{j \neq i, r_{ij} < r_c^{TB}} \left\{ 2Ap \exp\left[-p\left(\frac{r_{ij}}{r_0} - 1\right)\right] \right.$$

$$\left. -\frac{\xi q}{r_0} \left[\frac{1}{\sqrt{\text{E}_i^b}} + \frac{1}{\sqrt{\text{E}_j^b}}\right] \exp\left[-2q\left(\frac{r_{ij}}{r_0} - 1\right)\right] \right\} \frac{\boldsymbol{r}_{ij}}{r_{ij}} (2)$$

with

$$\text{E}_i^b = \sum_{j \neq i} \exp\left\{-2q\left(\frac{r_{ij}}{r_0} - 1\right)\right\} \qquad (3)$$

and

$$\text{E}_j^b = \sum_{k \neq j} \exp\left\{-2q\left(\frac{r_{jk}}{r_0} - 1\right)\right\} \qquad (4)$$

where r_0 is the first neighbour distance. For palladium $r_0 = 0.275$ nm. The interaction is cut off at $r_c^{TB} = 2.5 r_0$ (which includes neighbours up to the 5th). r_{ij} is the interatomic distance between i and j atoms. A, p, q, ξ are the TB-SMA parameters [22]. Even if this potential looks like a two-body form, it is needed for each j atom to search for all neighbours within the cutoff radius r_c^{TB} and to calculate the sum E_j^b, so non pairwise nature of the interactions become clear. This makes the calculations computer time consuming, especially when r_c^{TB} becomes quite large. While r_c^{TB} can be restricted to r_0 in bulk materials (because bulk atoms only oscillate at their equilibrium position), when deposition simulations are conducted, it is necessary to use larger cutoff radii, especially for accounting interactions with diffusing atoms. The value we choose is the smallest which does not change the results. It allows taking into account 92 neighbours (for palladium), each neighbour interacting with its own 92 neighbours (when comparing to bulk materials). For ultrathin films, the number of neighbours can only be reduced at initial steps. Thus it becomes clear that high performance (parallel) computers are required for treating long time deposition using such kind of interactions, which allows to treat a few thousands of incoming interacting particles with a few ten of thousand substrate atoms.

For interactions with fixed C atoms, we used a Lennard-Jones (LJ) 12 - 6 potential:

$$\boldsymbol{F}_i(\text{Pd}-\text{C}) = 24\,\varepsilon_{\text{Pd}-\text{C}} \sum_j \left\{ 2\left[\frac{\sigma_{\text{Pd}-\text{C}}}{r_{ij}}\right]^{12} - \left[\frac{\sigma_{\text{Pd}-\text{C}}}{r_{ij}}\right]^6 \right\} \frac{\boldsymbol{r}_{ij}}{r_{ij}^2} \qquad (5)$$

This Pd-C Lennard-Jones interaction potential is obtained by using the Lorentz-Berthelot mixing rule [16,25,26]: $\varepsilon_{\text{Pd}-\text{C}} = (\varepsilon_{\text{Pd}}\varepsilon_{\text{C}})^{\frac{1}{2}}$ and $\sigma_{\text{Pd}-\text{C}} = \frac{\sigma_{\text{Pd}}+\sigma_{\text{C}}}{2}$. The LJ Pd-Pd interaction

parameters are: $\varepsilon_{Pd} = 0.426$ eV and $\sigma_{Pd} = 0.252$ nm [27]. The parameters for C-C interactions can be found in reference [28] and the values are: $\varepsilon_C = 2.414\ 10^{-3}$ eV and $\sigma_C = 0.340$ nm. This gives: $\varepsilon_{Pd-C} = 0.02627$ eV and $\sigma_{Pd-C} = 0.299$ nm

The equations of motion are solved using the Verlet velocity algorithm [29,30]. A link-cell list is used to speed-up the computations in conjunction with Verlet lists for which radius $r_v = 2.7r_0$. Due to the non-pairwise interactions, the CPU time is not reduced to O(N), where N is the number of particles. The time step required for numerical integration of equations of motion is dt = 1 fs. It was verified it is enough up to impinging energy of 2 eV. For parallel implementation, we used the atom-decomposition scheme also known as replicated data method [31]. This method is used because the filling of space is expected not to be complete so spatial-decomposition scheme can not be an efficient scheme [31]. The parallel instruction library OpenMP has been found to be more efficient than message passing libraries as MPI because the calculations are performed on a shared memory supercomputer (SGI Origin 2000, 64 nodes, at CRIHAN, France). Briefly, N/p particles are treated by each p nodes during all the course of the simulation. At the same time, all information about each particle is known from each p nodes. Here p is varied from 4 to 14 depending on the load, so parallel efficiency is maintained above 90 %.

The simulated substrates are built from 3 atomic layers of 10.3 nm x 10.2 nm leading to rigid substrates of 12369 C atoms. This is sufficient for taking into account all interactions between incoming Pd atoms and substrate carbon atoms. In the following, one monolayer (ML) corresponds to 1521 atoms as for a Pd fcc (111) structure. Three kinds of surfaces have been built: an atomically smooth (surface C0); a highly roughened surface where atoms of the top layer are randomly displaced in-plane by 50% of the C-C distance, $a_{C-C} = 0.142$ nm , and 50% of the interlayer distance, $h_C = 0.335$ nm, perpendicular displacement (surface C1); and a flat surface with a localized defect of size $\approx$ 2nm (surface C2). This defect is composed of 60 carbon atoms 0.2 nm vertically elevated above their natural site. This latter structure is typical from ion or plasma irradiated surface [32,33]. These three surfaces are displayed in Fig. 1.

Each palladium atom are randomly launched every $\Delta t = 2$ ps above the surface. There are no interactions between Pd in the gas phase. All the Pd atoms interact simultaneously with other palladium atoms within the cutoff radius r_c^{TB} and with carbon rigid substrate atoms with a cutoff radius $r_c = 2.5\sigma_{Pd-C}$. The calculations have been performed at 0.31 ML (500 Pd atoms), 0.62 ML (1000 Pd atoms) and 0.93 ML (1500 Pd atoms), 1.08 ML (1750 atoms), 1.24 ML (2000 atoms), 1.40 ML (2250 atoms), 1.55 ML (2500 atoms), 1.71 ML (2750 atoms) and 1.86 ML (3000 atoms). Each set of calculation last for 6 ns (= 3000 atoms x 2 ps), for calculating interactions between 3000 incoming atoms among themselves and with 12369 substrate atoms. All sets of calculations use the same random number sequence. This means that differences between calculations for different surfaces or different energies will only originate from specific interactions.

The Pd initial mean kinetic energies are 0.026, 0.1 and 1. eV. In the former case, it simulates a metal vapor at $T_g = 300$ K. This occurs when sputtered Pd atoms travel across a buffer gas at sufficient pressure. When $T_g = 0.1$ eV, it is consistent with resistive or e-beam evaporation, which produces a vapor at the vaporisation temperature, which just lies in the range 0.1 eV. The latter case simulates a vapor at temperature $T_g = 1.0$ eV. This occurs for sputtering experiments at low pressure where a small amount of buffered gas only randomizes sputtered atom velocities, without not too much energy loss ($\approx$ 50%). Peak energy of the sputtered atom energy distribution is half vaporisation energy in vacuum (sputtered atom Thompson energy distribution). Then in all cases, initial velocities are chosen in Maxwell-Boltzmann distribution at the given temperature $T_g = 0.026$, 0.1 and 1.0 eV, with random corresponding incident angles.

For each surfaces C0, C1, C2 surfaces, three sets of deposition simulations are run corresponding to $T_g = 0.026$, 0.1 and 1.0 eV. Each run lasts 6 ns real time displaying 3000h CPU time shared by 4 to 14 processors on SGI Origin 2000 supercomputer (ILLIAC8 at CRIHAN). Altogether, calculations last 27000 hours corresponding to about 3 years on an equivalent single processor computer.

3 Results and discussion

The sticking coefficient is the ratio of the incoming atom number to the adsorbed atom number. It informs about adsorption processes [34]. Fig. 2. displays the evolution of the sticking coefficient for all conditions. The sticking is
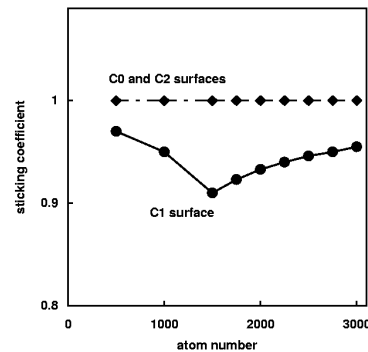

Fig. 2. Evolution of the sticking coefficient on surfaces C0, C1 and C2. Note it is independant from impinging kinetic energy

always unity except for surface C1, where it first decreases and then further increases. This behaviour is independant from the explored range of kinetic energy. Due to atomically sized roughness of surface C1, at low coverage, some

atoms ($\approx$ 5-10%) may not find a stable adsorption site and so desorbs. Then, sticking coefficient first decreases. When clusters are already formed and are stable enough, they offer a large capture area where sticking is unity. Thus it allows now to increase the sticking coefficient towards unity. That is the meaning of the initial decrease of sticking as plotted in Fig. 2.

On Fig 3-5 are plotted significant snapshots for the three surfaces at the three energies studied. In all cases,
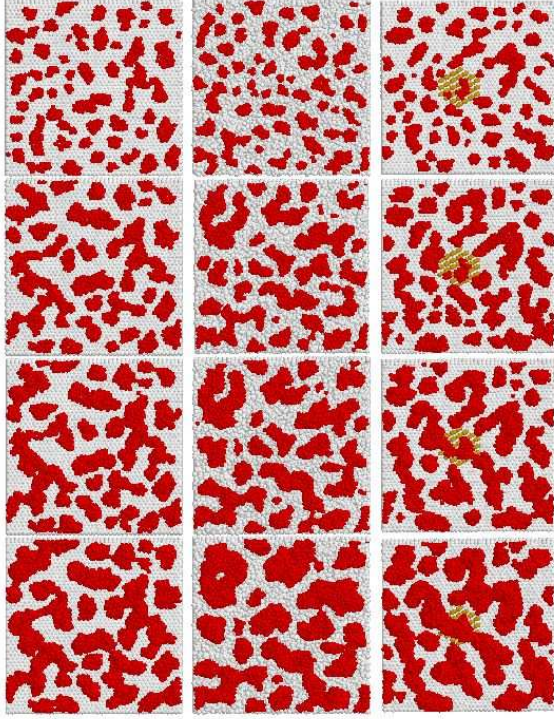
Fig. 3. Snapshots of Pd clusters deposited on surfaces C0 (left column), C1 (middle column) and C2 (right column). Size of imulated surfaces is 10.3 nm x 10.2 nm. The mean kinetic energy is $E_c = 0.026$ eV. From top to bottom the number of deposited atoms is respectively 1000, 1500, 2000 and 3000.

growth exhibit clusters which are more or less meandering. The cluster mean height is around 6 atom diameters (i.e. around 1.3 nm for Pd atoms) for 3000 deposited atoms (see Fig. 6). Looking at the shape of the clusters, we observe on Fig. 7 that clusters are more flat on rough surface C1 than on flat C0 and C2. In fact these two situations are reversed: clusters have rough top and flat bottom on the surfaces C0 and C2 compared to clusters that have flat top and rough bottom on the rough surface C1. This holds only for not too high clusters, i.e. when memory of growth starting conditions is kept. Moreover C1 clusters appear less ordered when looking at the edges (see Fig. 6). On a flat surface, first atomic layers in the clusters are parallel
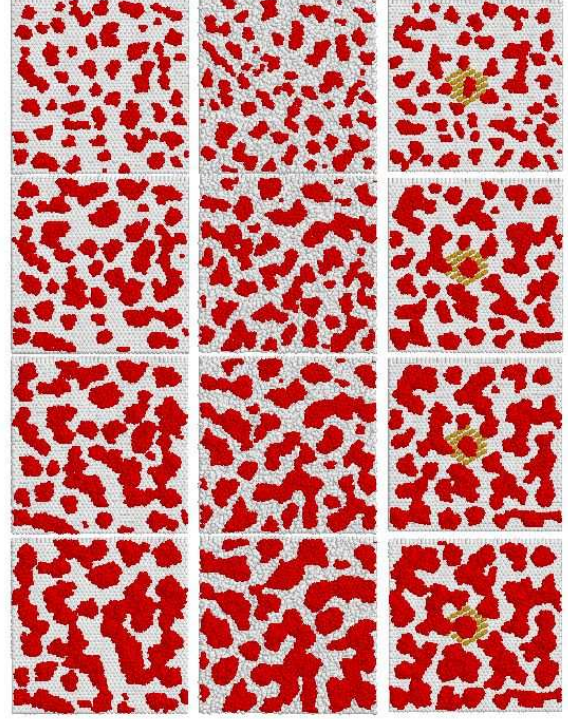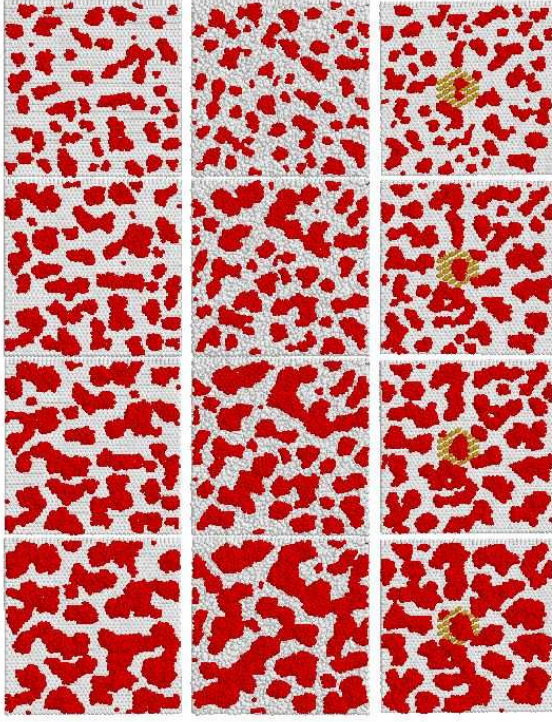

**Fig. 4.** same as Fig. 3 but for $E_c = 0.1$ eV

to the surface plane. On the contrary, clusters can not have the first layer parallel to a rough surface.

When looking at the same surface C0, C1 or C2 and examining cluster shapes at a fixed coverage, clusters become more compact (meandering has now a lower extent) as impinging atom kinetic energy increases. For example, surface C0 (left column of Fig. 3-5) for $E_c = 0.026$ eV has a more developed meandering structure than for E_c=1.0 eV. Moreover, for a 3000 incoming atom number the shape is quite different for the three energies while the cluster number remains the same (10 clusters when taking into account the cell periodicity). At fixed energy, and comparing among the three surfaces, differences appear essentially at high coverage. For low energy (Fig. 3), compacity is favoured on the rough surface. At highest energy no clear behaviour can be drawn.

Attention should also be paid to deposition on surface C2. Surface C2 differs from C0 only by the 60 elevated (0.2 nm) surface carbon atoms in its center. Simulations are done with the same random number sequence in each set of calculations. This allows direct comparison between results. Indeed, differences only originate from interactions due to the kind of surface. It is interesting to observe differences between surface C0 and C2 which come from the isolated defect. All the clusters on the whole surface are affected by the defect. Only pre-existing cluster on the defect (center of Fig. 3) is growing and enlarging on the

Fig. 5. same as Fig. 3 but for $E_c = 1.0$ eV
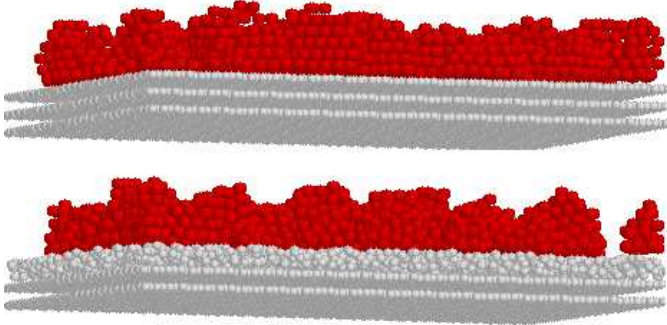
Fig. 6. Edges of cluster on surfaces C0 (top) and C1 (bottom)

defect. Other clusters remain at the edge of the defect. For the 1000 incoming atoms on Fig. 3, a cluster is disrupted by the edge of the defect. On C0, a larger cluster exists below the center of the simulation cell. On C2, one part on the cluster remains on the defect, the other one being located along the edge of the defect. For 3000 atoms deposited, small clusters are finally coalescing, bridging the defect. But the same long cluster does not exists on C0. This means that cluster-cluster interactions are also driven by the isolated defect. Highest kinetic energy does not overcome this effect. This can be due by a too high

kinetic barrier at the cluster edges i.e. diffusing atoms do not gain enough kinetic energy to climb on or over the defect. This is consistent with the experimental observation of step decoration on graphite. Fig. 5 also displays the same kind of differences in growth shapes between C0 and C1.
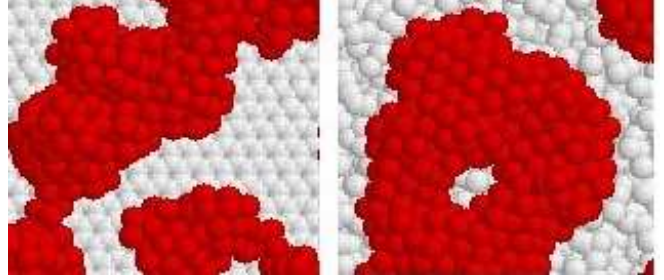
Fig. 7. Left picture is the surface of a cluster on flat graphite C0. The cluster outer surface is rough. On right picture, cluster on rough graphite C1, exhibits flatter surface

Informations that can be extracted from snapshots are cluster densities N_c, cluster mean sizes $\bar{d}$. The evolution against deposition time or equivalently impinging atom number N give information about growth modes [1,35,36,37].

Low coverage luster densities N_c are larger on the rough surface at the lowest kinetic energy. Increasing kinetic energy minimizes the effect of roughness on initial cluster density as can be seen in Table 1. When increas-

Table 1. Low coverage cluster densities N_c on surface C0, C1 and C2 for 500 deposited atoms

E_c (eV)	N_c on C0 (10^{12}cm^{-2})	N_c on C1 (10^{12}cm^{-2})	N_c on C2 (10^{12}cm^{-2})
0.026	64	73	65
0.10	65	69	69
1.00	61	69	65

ing deposition time the cluster densities are reduced and become independant of the roughness.

The evolution of the cluster mean size is often addressed in term of power laws. The most common growth power law is given by $\bar{d} \propto N^z$ for isolated clusters and $\bar{d} \propto N^{\alpha z}$ after cluster coalescence [37,38,39], N being the incoming atom number. z and αz are known as growth exponents and are deduced from statistical physics of growth phenomena. They were introduced for displaying common features of various phenomena in term of universal scaling laws. For addressing this question, we gather the mean areas $\bar{s}$ of the clusters at each energy and for each surface against all incoming atom numbers in Table 2. Note this area is the projected area perpendicular to the surface, thus it does not take into account the cluster height. This

is preferred because this is the same size that is deduced from electron microscopy pictures [5].

The evolution of the equivalent size $\bar{d}$ is recovered by $\bar{d} \propto \sqrt{\bar{s}}$ with $\bar{s} \propto N^{2\alpha z}$. We obtained values in the range $\alpha z = 0.75 - 0.87$ in agreement with Beysens et al [39] and Viovy et al [37] (In this case, $\alpha = 3$ [37]). This is consistent with static coalescence, i.e. clusters grow without moving until contact. It was also suggested that cluster growth could follow exponential law [40]. This is expected to occur when cluster diffusion takes place. Thus we also evaluate an exponential fit : $\bar{s} \propto e^{\mu N}$ in Table 2 with $\mu = 1.$ - 1.3. This means that some diffusion competes with static coalescence.

On surfaces C0 and C2, increasing energy results in larger cluster area at high coverage (> 1.5 ML) : increasing kinetic energy enhances the atom diffusion and diffusing atoms stick preferentially on the edges of large existing clusters even if they are far away. This effect also occurs because Pd cohesive energy is very high [1].

On rough surface, at high coverage, the largest areas are obtained for intermediate energy 0.1 eV. At the same time, lower cluster areas/sizes are obtained due to roughness which prevents sticking on too far cluster edges.

Power law behaviour (Table 2) confirms such analysis. Larger exponents (i.e. fastest growth kinetics) are obtained for higher energies on C0 and $2\alpha z = 1.75$. On C2 there is no dependence against kinetic energy, which again shows the special character of the C2 surface. For C1 it is obtained for the intermediate energy too and $2\alpha z = 1.7$. The meaning of this behaviour is not yet clear. One could expect that increasing energy above a threshold defined by the roughness scale first results in a behaviour similar to flat surface. But increasing again kinetic energy, result in hampered motion due to multiple interactions with atoms of the inhomogeneous surface. This would prevent further diffusion contrary to a flat surface. And cluster area/size decreases consequently. When considering exponential fit, inspection of snapshots from Fig. 3-5 shows that cluster deformation operates as cluster diffusion. Additional information is required for more precise statements about this question.

In Fig. 8 are plotted radial (or pair) distribution functions $g(r) = \frac{V}{N^2} * \sum_i \sum_{j \neq i} \delta(r - r_{ij})$ [30] for surface C0 and C1 at $E_c = 0.026$ and 1.00 eV This provides structural information about clusters, especially neighbour distances, ordering, ...(this is quite close to the information given by experimental EXAFS (Extended X-Ray Absorption Fine Structure)). Direct inspection of Fig. 8 shows that g(r) are composed of several peaks. These peaks give neighbour interatomic distances. Those corresponding to C0 are well defined and becomes narrower and numerous when increasing the number of deposited atoms. This means that long range order is taking place. This was already suggested by the fcc (111) good stacking displayed on the upper panel of Fig. 6.figure For C1, at all energies, peaks are broadened compared to C0, even for larger clusters. This means that ordering is not yet well established. This is in agreement with the observation of Fig. 6 where
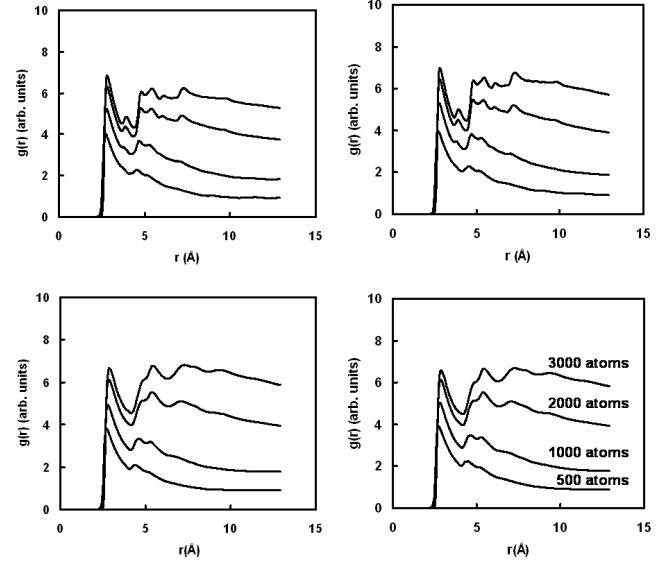
Fig. 8. Radial distribution functions for surfaces C0 and C1 at two energies.

clusters appear without any ordered stacking, contrary to C0. Moreover, the second and fifth neighbour peaks have disappeared, even for the highest deposited atom number. This means that the octaedral site characteristic of compact structure has disappeared. Recall that 2nd neighbours of an atom in a fcc (111) plane are located in upper (3 neighbours) and lower (3 neighbours) (111) planes. The in-plane disorder persists up to six atomic distances (which is the height of the clusters for 3000 deposited atoms). In Table 3 is reported the evolution of 1st r_n and 2nd r_{nn} neighbour distances for C0 surface and 1st r_n neighbour distance for C1. Recall that for fcc structures, $r_n = \frac{a_0}{\sqrt{2}}$ and $r_{nn} = a_0$, a_0 being the lattice parameter (a_0 = 0.389 nm for Pd). For bulk palladium $r_n = 0.275$ nm and $r_{nn} = a_0 = 0.389$ nm. Table 3 shows for both C0 and C1 surface departure from these values. At low coverage Pd atom find sites above the center of hexagonal ring of graphite. Such hexagons are separated by a distance of 0.246 nm (lattice parameter of graphite), thus at very low coverage when clusters are made of pair of atoms, r_n is closer to 0.246 nm rather than 0.275 nm. When increasing atom number, clusters grow and increase their closest atom distance. They crossed the ideal bulk value and a lattice expansion start as usual for nanometer sized clusters. For palladium deposition on MgO and for cluster size less than 2.5 nm lattice expansion as high as 0.8 % was found experimentally using grazing incidence small angle X-ray scattering [41]. For the C0 surface, at low coverage r_n and r_{nn} contraction is followed by further expansion. r_n is in the range 2.0%, while $r_{nn} = a_0$ expansion is only 0.5 %. The r_n value is fairly high, but cluster lowest size (cluster cross sectional size) is in the range 1.3 nm. For such low size, lattice behaviour could be very distorted. For C1, due to roughness induced mismatch, the r_n expansion is increased up to 4.9 %. But increasing energy

reduces r_n expansion to 3.8 %. This means that incoming atom kinetic energy assists growth in improving film density [11] by redistributing atoms in metastable sites created by atomic roughness of the substrate.

4 Conclusions

Molecular Dynamics simulations were conducted to study cluster growth on atomically ordered, disordered and defect ordered surfaces up to 2 monolayers (3000 atoms). We use rigid lattice approximation and quenched MD which is reasonable for deposition onto graphite surfaces. Cluster growth follows power law: $\bar{d} \propto t^{\alpha z}$, with $\alpha z = 0.75 - 0.87$. Influence of the type of disorder was investigated for different atom kinetic energies. The following trends are thus observed. It was shown that roughness can reduce sticking coefficients. Atomically flat cluster are obtained on rough surface at room temperature while clusters grown on atomically flat surface are rough. Roughness is also responsible for increasing low coverage cluster density and lattice expansion. Increasing kinetic energy of incoming atom tends to minimize these roughness effects. But localized defect play a role that is not smoothed by increasing kinetic energy: cluster growth is always disturbed by such a defect.

Acknowledgements

References

1. G. Venables, G. D. T. Spiller and M. Handbücken, *Rep. Prog. Phys.* **47**, 399 (1984)
2. A. Basillais, C. Boulmer-Leborgne, J. Mathias and J. Perrière, *Appl. Surf. Sci.* **186**, 416 (2002)
3. S. Esch, M. Breeman, M. Morgernstern, T. Michely and G. Comsa, *Surf. Sci.* **365**, 187 (1996)
4. A.-L. Thomann, J. P. Rozenbaum, P. Brault, C. Andreazza-Vignolle, and P. Andreazza, *Appl. Surf. Sci.* **158**, 172 (2000)
5. P. Brault, A.-L. Thomann, C. Andreazza-Vignolle, *Surf. Sci. Lett.* **406**, L597 (1998)
6. S. M. Rossnagel *IBM Journal of Research & Development* **43**, 163 (1999)
7. B. Chapman *Glow Discharge Process* (New York, Wiley, 1980); D. L. Smith *Thin Film Deposition* (New York: Mc Graw Hill, 1995)
8. G. H. Gilmer, H. Huang and C. Roland *Comp. Mat. Sci.* **23**, 354 (1998)
9. G. H. Gilmer, H. Huang and T. Diaz de la Rubia, J. Dalla Torre, and F. Baumann *Thin Solid Films* **365**, 189 (2000)
10. H. N. G. Wadley, X. Zhou, R. A. Johnson and M. A. Neurock, *Progress in Materials Science* **46**, 329 (2001)
11. K. H. Müller, *J. Appl. Phys.* **59**, 2803 (1986); K. H. Müller, *J. Vac. Sci. Technol. A* **4**, 184 (1986)
12. K. H. Müller, *Phys. Rev. B* **35**, 7906 (1987)
13. R. W. Smith, and D. J. Srolovitz, *J. Appl. Phys.* **79**, 1448 (1996)
14. L. Dong, R. W. Smith, and D. J. Srolovitz, *J. Appl. Phys.* **80**, 5682 (1996)
15. P. Brault, A.-L. Thomann, C. Andreazza-Vignolle, and P. Andreazza *Eur. Phys. J. AP* **19**, 83 (2002)
16. W. D. Luedtke and U. Landmann, *Phys. Rev. B* **40**, 11733 (1989)
17. L. Lewis and R. M. Niemenen, *Phys. Rev. B* **54**, 1459 (1996)
18. L. Lewis, P. Jensen, and J. L. Barrat, *Phys. Rev. B* **56**, 2248 (1997)
19. M. H. Shapiro *Surf. Coat. Technol.* **103-104**, 1 (1998)
20. M. S. Daw and M. I. Baskes, *Phys. Rev. B* **29**, 1289 (1984); M. S. Daw, S. M. Foiles and M. I. Baskes, *Materials Science Reports* **9**, 251 (1993)
21. Desjonquères M C and Spanjaard D *Concepts in Surface Physics* (Berlin: Springer Verlag, 1998)
22. V. Rosato, M. Guillope and B. Legrand, *Phil. Mag. A* **59**, 321 (1989)
23. B. Legrand and G. Tréglia *Surf. Sci.* **236**, 398 (1990)
24. C. Mottet, G. Tréglia, B. Legrand, *Phys. Rev. B* **46** ,16018 (1992)
25. S. Y. Liem, S. K. Chan, R. F. Savinell, *Molecular Simulation* **13**, 47 (1994)
26. Wu G W, Chan K Y 1996 *Surf. Sci.* **365** 38
27. T. Halicioglu and G. M. Pound, *Phys. Stat Sol. (a)* **30** 619 (1975)
28. W. A. Steele, *Surf. Sci.* **36**, 317 (1973)
29. W. C. Swope, H. C. Andersen, P. H. Berens and K. R. Wilson, *J. Chem. Phys.* **76** , 637 (1982)
30. M. P. Allen and D. J. Tildesley *Computer Simulations of Liquids* (Oxford: Clarendon Press, 1987)
31. S. J. Plimpton, *J. Comp. Phys.* **117**, 1 (1996)
32. J. R. Hahn and H. Kang, *Phys. Rev. B* **60**, 6007 (1999)
33. B. Rousseau, H. Estrade-Szwarckopf, A.-L. Thomann, and P. Brault, *Appl. Phys. A* 77, 591 (2003)
34. P. Brault, H. Range, J. P. Toennies, *J. Chem. Phys.* **106**, 8876 (1997)
35. M. Zinke-Allmang, M. C. Feldmann, M. H. Grabow, *Surf. Sci. Rep.* **16** 377 (1992)
36. P. Meakin, *Phys. Rep.* **235**, 189 (1993)
37. J. L. Viovy, D. Beysens, and C. M. Knobler *Phys. Rev. A* **37** 4965 (1988)
38. F. Family and P. Meakin, *Phys. Rev. A* **40**, 3836 (1989)
39. D. Beysens, C. M. Knobler and H. Schaffar, *Phys. Rev. B* **41**, 9814 (1990)
40. P. Jensen, L. Barabási, H. Larralde, S. Havlin, and H. E. Stanley *Phys. Rev. B* **50**, 15316 (1994)
41. H. Fornander, J. Birch, L. Hultman, L. G. Petersson, and J. E. Sundgren *Appl. Phys. Lett.* **68** 2636 (1996)
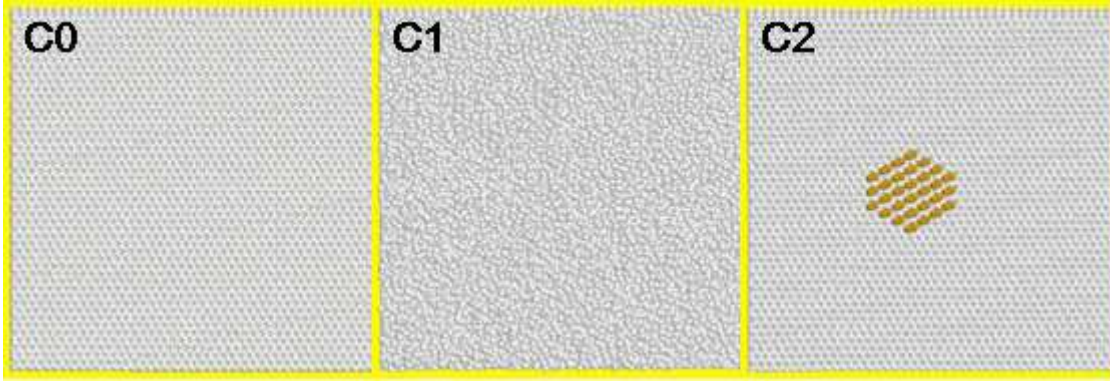
Fig. 1. Simulated graphite surfaces (10.3 nm x 10.2 nm): C0, atomically flat; C1, with randomly disordered first outer plane; C2, flat with a localized defect. The defect is dark gray

Table 2. Cluster area $\bar{s}$ (nm^2) evolution against incoming atom number N for the three surfaces C0, C1,C2 and the mean kinetic energies 0.026, 0.1, 1.0 eV. Two kinds of fit are displayed : $\bar{s} \propto N^{2\alpha z}$ and $\bar{s} \propto e^{\mu N}$. Values between brackets give a less good fit than power law does.

surface	C0 $\bar{s}$ (nm^2)			C1 $\bar{s}$ (nm^2)			C2 $\bar{s}$ (nm^2)		
N	0.026	0.10	1.00	0.026	0.10	1.00	0.026	0.10	1.00
500	0.31	0.31	0.34	0.26	0.28	0.28	0.31	0.30	0.31
1000	0.68	0.68	0.70	0.57	0.59	0.66	0.68	0.75	0.99
1500	1.64	1.46	1.40	1.77	0.95	1.27	1.62	1.56	1.90
1750	2.15	1.61	2.07	1.77	1.80	1.67	2.23	2.09	2.19
2000	2.91	2.13	2.93	2.19	2.13	1.81	3.03	2.49	2.54
2250	3.39	2.83	3.59	2.51	2.46	2.05	3.28	3.24	3.54
2500	3.28	3.42	4.92	3.03	3.49	2.56	4.20	3.40	3.89
2750	3.84	4.38	6.17	3.17	4.39	3.53	4.30	4.51	4.32
3000	5.09	5.75	5.71	3.96	5.92	5.41	6.35	4.41	4.82
$2\alpha z$	1.6	1.6	1.75	1.5	1.7	1.5	1.6	1.6	1.5
μ	(1.)	1.1	1.3	(1.)	1.2	1.1	(1.)	(1.)	(1.)

Table 3. First r_n and second r_{nn} neighbour distance for all deposited atom numbers N and for surface C0 and C1.

surface	C0 E_c (eV)			C0 E_c (eV)			C1 E_c (eV)		
N	0.026	0.10	1.00	0.026	0.10	1.00	0.026	0.10	1.00
	r_n (nm)			r_{nn} (nm)			r_n (nm)		
500	0.2688	0.2710	0.2710	0.3650	0.3661	-	0.2710	0.2715	0.2721
1000	0.2754	0.2743	0.2754	0.3759	0.3759	0.3792	0.2765	0.2798	0.2787
1500	0.2787	0.2787	0.2776	0.3825	0.3857	0.3836	0.2819	0.2819	0.2841
1750	0.2798	0.2776	0.2787	0.3857	0.3868	0.3857	0.2819	0.2841	0.2852
2000	0.2809	0.2808	0.2798	0.3868	0.3879	0.3901	0.2852	0.2852	0.2852
2250	0.2798	0.2808	0.2819	0.3879	0.3890	0.3920	0.2874	0.2852	0.2852
2500	0.2808	0.2808	0.2808	0.3912	0.3901	0.3901	0.2885	0.2874	0.2874
2750	0.2808	0.2808	0.2808	0.3901	0.3912	0.3901	0.2885	0.2874	0.2852
3000	0.2808	0.2808	0.2808	0.3923	0.3912	0.3901	0.2885	0.2874	0.2852